Int J Thermophys (2008) 29:434–444
DOI 10.1007/s10765-007-0300-1

Thermophysical Properties of a Chromium–Nickel–Molybdenum Steel in the Solid and Liquid Phases

B. Wilthan · H. Reschab · R. Tanzer · W. Schützenhöfer · Gernot Pottlacher

Published online: 6 November 2007

Abstract Numerical simulation of vacuum arc re-melting, pressurized or protective electro-slag re-melting, and ingot casting have become quite important in the metal industry. However, a major drawback of these simulation techniques is the lack of accurate thermophysical properties for temperatures above 1,500 K. Heat capacity, heat of fusion, density, and thermal conductivity are important input parameters for the heat transfer equation. Since, direct measurements of thermal conductivity of alloys in the liquid state are almost impossible, its estimation from electrical conductivity using the Wiedemann–Franz law is very useful. The afore-mentioned thermophysical properties of several steels are investigated within the context of an ongoing project. Here, we present a full set of thermophysical data for the chromium–nickel–molybdenum steel meeting the standard DIN 1.4435 (X2CrNiMo18-14-3); these values will be used by our partner to simulate various re-melting and solidification processes. Wire-shaped samples of the steel are resistively volume-heated, as part of a fast capacitor discharge circuit. Time-resolved measurements with sub-μs resolution of current through the specimen are performed with a Pearson probe. The voltage drop across the specimen is measured with knife-edge contacts and ohmic voltage dividers, the temperature of the sample with a pyrometer, and the volumetric expansion of the wire with a fast acting CCD camera. These measurements enable the heat of fusion, the heat capacity, and the electrical resistivity to be determined as a function of temperature in the solid and liquid phases. The thermal conductivity and thermal diffusivity are estimated via the Wiedemann–Franz law.

B. Wilthan · H. Reschab · G. Pottlacher (✉)
Institut für Experimentalphysik, Technische Universität Graz, Petersgasse 16, 8010 Graz, Austria
e-mail: pottlacher@tugraz.at

R. Tanzer · W. Schützenhöfer
Böhler Edelstahl GmbH & Co KG, Mariazellerstrasse 25, 8605 Kapfenberg, Austria

Keywords DIN 1.4435 · Enthalpy · Pulse-heating · Resistivity · Thermal conductivity · Thermal diffusivity · Thermophysical properties

1 Introduction

The chemical composition of the investigated stable austenitic steel DIN 1.4435 (see also Table 1) is optimized for applications, where a homogeneous structure of the metal is required.

Due to the high amount of chromium, nickel, and molybdenum and the low carbon content, this alloy is very resistant to intergranular corrosion in the temperature range up to 673 K. Its resistance to acids having a reducing effect (e.g., dilute sulfuric acid and hydrochloric acid) is good. For optimum resistance, surfaces should be pickled. The steel is not susceptible to pitting, nor to crevice and stress corrosion cracking, in media containing chloride ions, and it possesses excellent resistance to attack from urea. This steel is weldable with analogous filler metal giving fully austenitic deposit and does not require post-weld heat treatment. Cold forming properties are good. The steel is capable of taking a mirror finish.

Products made of this steel grade include components for urea plants, pump heads, valve stems, condensers, and reactors, as well as equipment and parts in the dyeing, textile, paper, leather, pharmaceutical, chemical, and synthetic fiber industries.

2 Measurements

A fast ohmic pulse-heating technique is applied to wire-shaped samples with a diameter of about 0.65 mm and a typical length of 70 mm. Samples with the chemical composition given in Table 1 were provided by our partner, Böhler Edelstahl GmbH & Co KG. The solidus and liquidus temperatures were determined by them to be $T_s = 1{,}701$ K (index s: solidus) and $T_l = 1{,}762$ K (index l: liquidus).

During our experiment, the sample is heated from room temperature to the liquid phase within a few μs during which time the thermophysical properties in the solid and liquid states are measured. Time resolved electrical measurements of the current through the wire and the voltage drop across a defined active length are collected. Calculations of the enthalpy and electrical resistivity take into account the sample mass. Simultaneous optical measurements of the surface radiance of the sample determine the temperature by means of Planck's law. In order to obtain the volume expansion of the sample, the silhouette of the wire is captured by a specially designed

Table 1 Chemical composition and comparable standards of the X2CrNiMo18-14-3 (DIN 1.4435) steel

Chemical composition (average %)							
Fe	Cr	Ni	Mo	Mn	Si	N	C
Bal.	17.50	14.50	2.70	1.70	0.30	0.07	max. 0.030
Comparable standards							
AISI	UNS	JIS		UNI		GOST	
∼316L	∼S31603	SUS 316L		∼X2CrNiMo17-3		∼03Ch16N15M3	

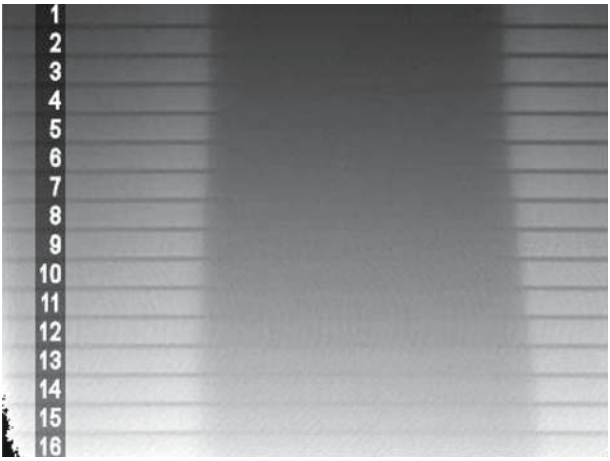

Fig. 1 Change of diameter of the wire sample during the experiment from room temperature at image 1 to the end of the liquid phase at image 16, detected with 16 rows of pixels of a fast CCD-Camera every 4.98 μs

fast-acting framing CCD-array. Figure 1 shows a picture with 16 frames in a row. Starting with the top frame at room temperature and initial geometry, the second frame shows the same spot on the sample after 4.98 μs. The time interval between two consecutive frames is adjustable and was always set to 4.98 μs for these experiments. Thus, sample expansion as a function of temperature is experimentally determined, and density as a function of temperature might be calculated by combining the thermal expansivity with the known density at room temperature. The thermal diffusivity is then estimated via the Wiedemann–Franz law.

A differential-scanning calorimeter (DSC) Netzsch DSC 404 is used to perform accurate specific-heat-capacity measurements in the temperature range from 500 to 1,500 K. The DSC results are combined with those of the pulse-heating experiments by using the temperature-dependent enthalpy data from the DSC to expand the temperature range of the pulse-heating data. Thus, the temperature dependences of all thermophysical properties may be extended to the DSC onset temperature of about 500 K.

Based on all of the measured data, thermophysical properties such as enthalpy, specific heat capacity, resistivity, density, thermal conductivity, and thermal diffusivity (all functions of temperature) are presented in the following sections for the solid and liquid states of this X2CrNiMo18-14-3 steel.

For further information on the pulse heating circuit and the DSC, as well as for more details of the data evaluation, see [1]. Information regarding the CCD-Camera is given in [2].

3 Results

The specific enthalpy H versus temperature T is presented in Fig. 2, wherein the enthalpy at room temperature (298 K) is the zero of the pulse heating experiment. In

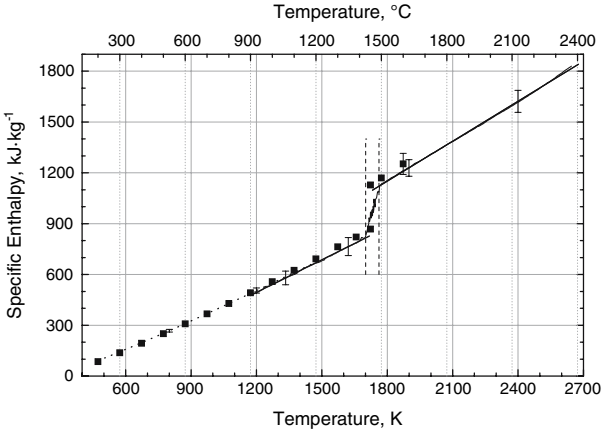

Fig. 2 Specific enthalpy in the solid and liquid state. *Vertical dashed lines*: solidus and liquidus temperatures; *dotted line*: data from DSC-measurement (Eq. 1); *bold lines*: fit for the solid phase (Eq. 2) and fit for the liquid phase (Eq. 3) from the data of the pulse-heating experiments; and *squares*: recommended values for the similar stainless steel Fe-316 from Mills [3]

industrial applications, temperatures in °C are often used; for this reason both K and °C are given in the figures. The enthalpy data from the DSC-measurements are given by Eq. 1. An average of 11 pulse-heating measurements delivers the linear fit for the solid (Eq. 2) and liquid (Eq. 3) states, with the enthalpy expressed in $\mathrm{kJ}\cdot\mathrm{kg}^{-1}$ and the temperature in K.

$$H(T) = -149.5 + 0.4798T + 5.41 \times 10^{-5}\,T^2 \qquad 500\,\mathrm{K} < T < 1{,}500\,\mathrm{K} \qquad (1)$$

$$H(T) = -277.2 + 0.6425T \qquad 1{,}200\,\mathrm{K} < T < 1{,}701\,\mathrm{K} \qquad (2)$$

$$H(T) = -266.3 + 0.7870T \qquad 1{,}762\,\mathrm{K} < T < 2{,}650\,\mathrm{K} \qquad (3)$$

From solidus to liquidus, indicated in Fig. 2 by vertical dashed lines, the specific enthalpy changes from $H(T_\mathrm{s}) = 816\,\mathrm{kJ}\cdot\mathrm{kg}^{-1}$ to $H(T_\mathrm{l}) = 1{,}120\,\mathrm{kJ}\cdot\mathrm{kg}^{-1}$, yielding $\Delta H = 304\,\mathrm{kJ}\cdot\mathrm{kg}^{-1}$ for the latent heat of fusion.

We obtain c_p values of $643\,\mathrm{J}\cdot\mathrm{kg}^{-1}\cdot\mathrm{K}^{-1}$ for the end of the solid state and $787\,\mathrm{J}\cdot\mathrm{kg}^{-1}\cdot\mathrm{K}^{-1}$ for the liquid state from the slope of $H(T)$ during the pulse heating experiments. The specific heat capacity in Fig. 3 was measured with the high temperature calorimeter. The open circles represent data from our own measurements as listed in Table 2.

The density d at room temperature was determined by fabricating a cylinder with maximum machine accuracy with the approximate dimensions of 50-mm diameter and 50-mm height, then measuring and weighing it. The calculated value for the density of the investigated steel is $7{,}986\,\mathrm{kg}\cdot\mathrm{m}^{-3}$ at room temperature. The density as a function of temperature is shown in Fig. 4 (right-hand scale). The measured values for the change of volume V/V_0, obtained by fast pulse heating, are indicated as circles corresponding to the left-hand scale in the figure. The polynomial fits for the pulse-heated results for

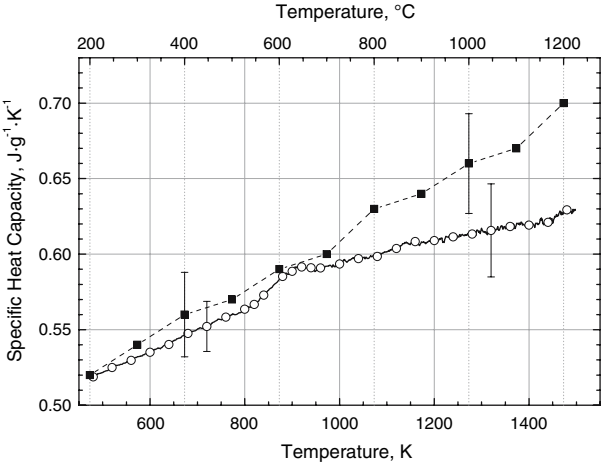

Fig. 3 Specific heat capacity measured with a differential scanning calorimeter as a function of temperature. *Circles*: measured data—values of the marked data points are given in Table 2 and *squares*: recommended values for a similar stainless steel Fe-316 from Mills [3]

Table 2 Data for specific heat of the solid-steel X2CrNiMo188-14-3 (DIN 1.4435) from DSC measurements

T (K)	c_p ($J \cdot g^{-1} \cdot K^{-1}$)	T (K)	c_p ($J \cdot g^{-1} \cdot K^{-1}$)	T (K)	c_p ($J \cdot g^{-1} \cdot K^{-1}$)
480	0.519	840	0.573	1,160	0.608
520	0.525	880	0.585	1,200	0.609
560	0.530	900	0.589	1,240	0.612
600	0.535	920	0.592	1,280	0.613
640	0.540	940	0.591	1,320	0.616
680	0.548	960	0.591	1,360	0.618
720	0.552	1,000	0.594	1,400	0.619
760	0.558	1,040	0.597	1,440	0.621
800	0.564	1,080	0.599	1,480	0.629
820	0.567	1,120	0.604		

the change of volume are given by Eqs. 4 and 5:

$$V/V_0(T) = 0.997 + 5.7 \times 10^{-6}T + 2.0 \times 10^{-8}T^2 \quad 1{,}200\,\mathrm{K} < T < 1{,}701\,\mathrm{K} \quad (4)$$

$$V/V_0(T) = 0.855 + 1.33 \times 10^{-4}T \quad 1{,}762\,\mathrm{K} < T < 2{,}300\,\mathrm{K} \quad (5)$$

In calculating the polynomial for the solid phase, the value of $V/V_0 = 1$ at room temperature was also taken into account. Equations 6 and 7 represent the density as a function of temperature; d is in $kg \cdot m^{-3}$ and T is in K.

$$d(T) = 8{,}050 - 0.124T - 1.17 \times 10^{-4}T^2 \quad 1{,}200\,\mathrm{K} < T < 1{,}701\,\mathrm{K} \quad (6)$$

$$d(T) = 9{,}213 - 1.243T + 9.9 \times 10^{-5}T^2 \quad 1{,}762\,\mathrm{K} < T < 2{,}300\,\mathrm{K} \quad (7)$$

From room temperature up to the solidus, this work reports a decrease in density of 6.1%.

The specific electrical resistivity ρ of the investigated steel is presented in Fig. 5 as a function of temperature. The lower branch of curves represents data for the initial geometry (index IG, no compensation for thermal expansion), whereas the upper values are the resistivity recalculated by taking into account the change of volume (index CO, compensation for volume expansion). Temperature-dependent data from pulse heating are only available above the lowest working temperature of our pyrometer, which operates at a wavelength of 1,570 nm and has a bandwidth (FWHM) of 84 nm. For the data (Eqs. 8, 9) depicted as dotted lines, the electrical signals during the pulse-heating are merged with temperature data from the DSC measurement via enthalpy; for details, see also [1].

$$\rho_{\mathrm{IG}}(T) = 0.567 + 9.87 \times 10^{-4} T - 5.11 \times 10^{-7} T^2 + 9.67 \times 10^{-11} T^3 \quad 500\,\mathrm{K} < T < 1{,}500\,\mathrm{K} \tag{8}$$

$$\rho_{\mathrm{CO}}(T) = 0.566 + 9.79 \times 10^{-4} T - 4.75 \times 10^{-7} T^2 + 9.5 \times 10^{-11} T^3 \quad 500\,\mathrm{K} < T < 1{,}500\,\mathrm{K} \tag{9}$$

At the solidus, indicated by a vertical dashed line, we obtain, for the resistivity corresponding to the initial geometry ρ_{IG} a value of $1.24\,\mu\Omega \cdot \mathrm{m}$, and at the liquidus, a value of $1.27\,\mu\Omega \cdot \mathrm{m}$; thus, an increase of $\Delta\rho_{\mathrm{IG}} = 0.03\,\mu\Omega \cdot \mathrm{m}$ is observed at melting. The corresponding fits are Eqs. 10 and 11.

$$\rho_{\mathrm{IG}}(T) = 0.919 + 2.97 \times 10^{-4} T - 6.3 \times 10^{-8} T^2 \quad 1{,}200\,\mathrm{K} < T < 1{,}701\,\mathrm{K} \tag{10}$$

$$\rho_{\mathrm{IG}}(T) = 1.2967 - 3.81 \times 10^{-5} T + 1.29 \times 10^{-8} T^2 \quad 1{,}762\,\mathrm{K} < T < 2{,}650\,\mathrm{K} \tag{11}$$

When the electrical resistivity is corrected for thermal expansion, we obtain higher values. At the solidus, we obtain a value of $1.32\,\mu\Omega \cdot \mathrm{m}$ (Eq. 12), and at the liquidus a value of $1.38\,\mu\Omega \cdot \mathrm{m}$ (Eq. 13). Thus, an increase of $\Delta\rho_{\mathrm{CO}} = 0.06\,\mu\Omega \cdot \mathrm{m}$ is observed at melting.

$$\rho_{\mathrm{CO}}(T) = 0.916 + 2.97 \times 10^{-4} T - 3.4 \times 10^{-8} T^2 \quad 1{,}200\,\mathrm{K} < T < 1{,}701\,\mathrm{K} \tag{12}$$

$$\rho_{\mathrm{CO}}(T) = 1.1269 + 1.148 \times 10^{-4} T + 1.74 \times 10^{-8} T^2 \quad 1{,}762\,\mathrm{K} < T < 2{,}300\,\mathrm{K} \tag{13}$$

Figure 6 presents the thermal conductivity, λ, and thermal diffusivity, a, versus temperature. In order to estimate the thermal conductivity via the Wiedemann–Franz law (see [7]), the electrical resistivity compensated for thermal expansion of the sample (ρ_{CO}) must be used. For this reason, the temperature range in the liquid phase is limited by the density data. At the onset of melting, we obtain a value for λ of $31.6\,\mathrm{W} \cdot \mathrm{m}^{-1} \cdot \mathrm{K}^{-1}$ and at the end of melting (for the beginning of the liquid phase)

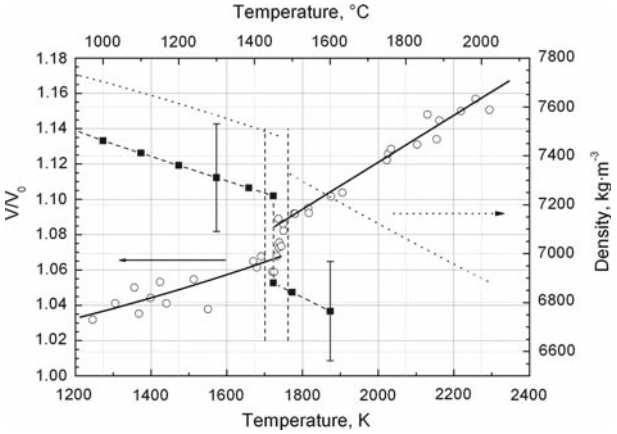

Fig. 4 Change of volume (left scale) and density (right scale) as a function of temperature. *Circles*: measured data points; *bold lines*: fits for the data points of change of volume with (Eq. 4) for the solid phase and (Eq. 5) for the liquid phase; *dotted lines*: fit for the density in the solid (Eq. 6) and liquid (Eq. 7) phases; *squares*: recommended values for the similar stainless steel Fe-316 from Mills [3]; and *vertical dashed lines*: solidus and liquidus temperatures

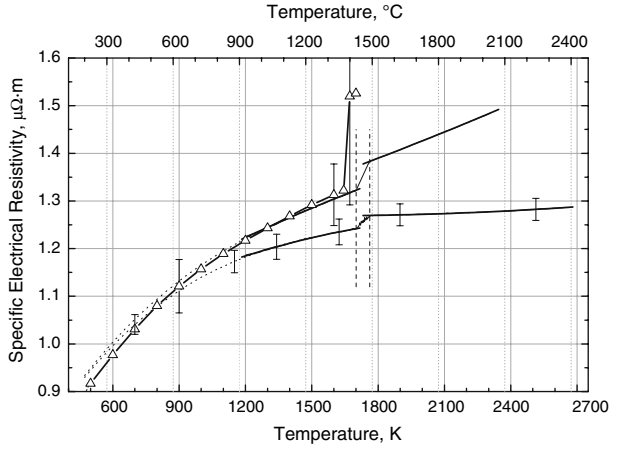

Fig. 5 Specific electrical resistivity versus temperature. Lower set of curves represents resistivity assuming the initial geometry; upper dataset gives the values corrected for the change of volume. *Dotted lines*: electrical values from pulse heating— temperature from DSC measurement; *bold solid lines*: fits to the experimental data from pulse heating; *triangles*: recommended values for the similar stainless steel AISI 316 from Chu and Ho [4]; and *vertical dashed line*: solidus (1,701 K) and liquidus (1,762 K) temperatures

a value of $31.3\,\mathrm{W}\cdot\mathrm{m}^{-1}\cdot\mathrm{K}^{-1}$. The corresponding least-squares polynomials obtained within this work for thermal conductivity in the solid phase and the liquid phase are listed in Eqs. 14–16. In Pehlke et al. [5], a value of $\lambda = 31.86\,\mathrm{W}\cdot\mathrm{m}^{-1}\cdot\mathrm{K}^{-1}$ is given for the end of the solid phase of the stainless steel AISI 316, a comparable standard with

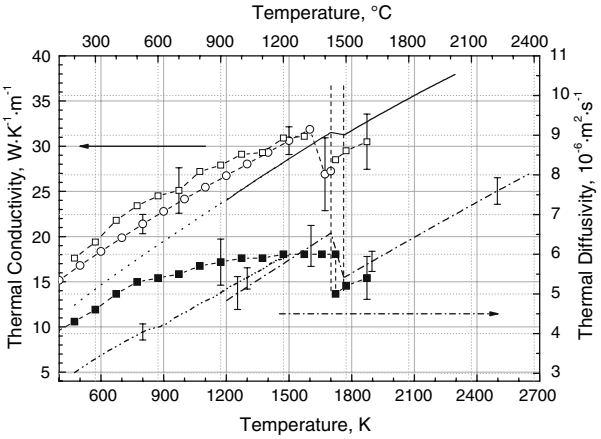

Fig. 6 Thermal conductivity (λ) and thermal diffusivity (a) versus temperature in the solid and liquid states. *Vertical dashed lines*: solidus and liquidus temperature; *circles*: literature values of λ for the steel AISI 316 [5]; *open squares*: data for λ for the similar stainless steel Fe-316 from Mills [3]; *dotted line*: λ calculated from (9); full line: λ calculated from pulse heating data, e.g., (12,13); *dashed-dotted-dotted line*: a calculated with DSC data; *dashed-dotted line*: a only from pulse heating data; and *full squares*: data for a for the similar stainless steel Fe-316 from Mills [3]

respect to the alloy composition.

$$\lambda(T) = 4.35 + 1.782 \times 10^{-2} T - 1.13 \times 10^{-6} T^2 \qquad 500\,\mathrm{K} < T < 1{,}500\,\mathrm{K} \quad (14)$$

$$\lambda(T) = 6.26 + 1.489 \times 10^{-2} T \qquad 1{,}200\,\mathrm{K} < T < 1{,}701\,\mathrm{K} \quad (15)$$

$$\lambda(T) = 9.04 + 1.263 \times 10^{-2} T \qquad 1{,}762\,\mathrm{K} < T < 2{,}300\,\mathrm{K} \quad (16)$$

Calculation of the thermal diffusivity, a, is based on the validity of the Wiedemann–Franz relationship within the stated temperature range. At the onset of melting, we obtain a value for a of $6.54 \times 10^{-6}\,\mathrm{m^2 \cdot s^{-1}}$ and at the end of melting (the beginning of the liquid phase) a value of $5.42 \times 10^{-6}\,\mathrm{m^2 \cdot s^{-1}}$.

$$a(T) = 1.74 + 2.82 \times 10^{-3} T \quad 500\,\mathrm{K} < T < 1{,}500\,\mathrm{K} \quad (17)$$

$$a(T) = 0.77 + 3.39 \times 10^{-3} T \quad 1{,}200\,\mathrm{K} < T < 1{,}701\,\mathrm{K} \quad (18)$$

$$a(T) = 0.22 + 2.95 \times 10^{-3} T \quad 1{,}762\,\mathrm{K} < T < 2{,}650\,\mathrm{K} \quad (19)$$

4 Discussion

The investigated steel X2CrNiMo18-14-3 is austenitic and face-centered-cubic (fcc) throughout the solid phase, with the dissolved Ni functioning as an austenite stabilizer. The DSC measurements show that c_p deviates a little from a straight line within the temperature range from 800 to 1,000 K, where a little endothermic dip is observed that might arise from minor precipitations during the heat treatment of the production

process. Mills [3] recommends values of c_p for a similar stainless steel (316), which are plotted as squares in Fig. 3. Up to 1,000 K, both curves are identical within the stated uncertainties. At higher temperatures, the slope of the literature data is higher, but the difference in c_p never exceeds 10%. Literature values for the specific enthalpy depicted in Fig. 2 show identical values for the solid and very good agreement for the liquid phase. The measured enthalpy of melting of $304\,\mathrm{kJ \cdot kg^{-1}}$ agrees well with the value of $307\,\mathrm{kJ \cdot kg^{-1}}$ given in [3].

The thermal diffusivity in Fig. 6 shows a non-linear behavior in this temperature range. This results from the direct mathematical interrelationship of a with the specific heat capacity in the Wiedemann–Franz law. Using a direct method (e.g., a laser flash apparatus), it is expected that this deviation might not appear. Thus, the thermal diffusivity is described by a linear dependence, see Eq. 17, with adequate accuracy.

Experimental data for the change of volume are only available up to 2,300 K. The mechanical stability of this material in the liquid phase at high temperatures limits the quality of the images collected with the method used. Hence, corrections for the change of volume required to calculate the specific electrical resistivity and the thermal conductivity are also limited to 2,300 K. Between room temperature and the first data points for thermal expansion of the wire at 1,200 K, the interpolation of Eq. 6 is used to calculate the resistivity data including the change of volume as given in Eq. 9. Mills [3] shows lower values for the density in the solid and liquid phases. A levitated drop method was used to collect the recommended density data.

The recommended resistivity data from Chu and Ho [4] is in perfect agreement with the measured data for the solid phase. For the liquid phase, the uncertainty of the literature data for ρ is too large to form an opinion about the two reported data points.

In order to compare literature values of thermal conductivity with those for the material of Fig. 6, it is necessary to recognize that the chemical composition is not exactly the same, although it is in the same range. Further, calculations with the Wiedemann–Franz law only consider the electronic contribution to the thermal conductivity. According to Klemens and Williams [6], there is also a constant contribution from the lattice to consider. It is suspected that the differences between the literature values and the measured data are due to the neglected phonon contribution. In [6], a value of $1.031\,\mu\Omega \cdot \mathrm{m}$ is given for the electrical resistivity of the stainless steel 316, which is similar in chemical composition to the material under investigation. For thermal conductivity, Klemens reports $19.9\,\mathrm{W \cdot m^{-1} \cdot K^{-1}}$ at 700 K, of which $4.9\,\mathrm{W \cdot m^{-1} \cdot K^{-1}}$ are due to the lattice contribution. These data agree well with the thermal conductivity reported here for this temperature. Further investigations concerning this topic will be undertaken within a new project.

The measured values for a are in good agreement with literature values within the stated uncertainties for temperatures above 1,400 K. Below this temperature, the literature reports higher values.

5 Uncertainties

The stated uncertainties correspond to a single experiment, and have been calculated using the Guide to the Expression of Uncertainty in Measurement (GUM) [8]. For the

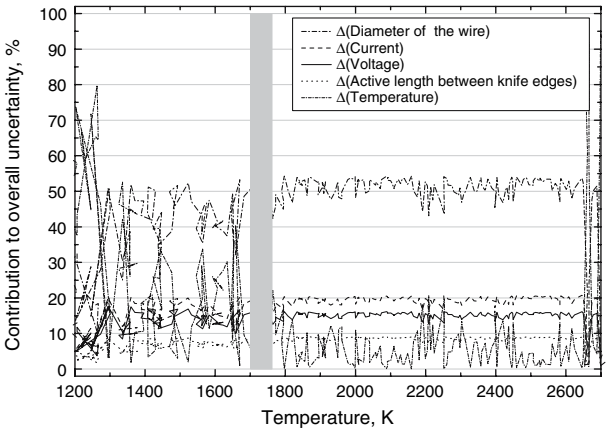

Fig. 7 Contribution to the overall uncertainty of the specific electrical resistivity from the measured quantities. *Gray bar* marks the melting range of the alloy

measured quantities of the pulse-heating experiment (diameter of the wire, current, voltage drop, and temperature), uncertainties based on calibration certificates or operating manuals of the measuring boards were used as input values for the calculation of uncertainty.

The uncertainty of the pyrometrically determined temperature was calculated with respect to the temperature dependence of the calibration constant, the melting temperature of the alloy, the effective wavelength of the filter, the adjustment to the probe, the specification of the measuring board, and a theoretical estimation of the temperature difference between the center and the surface of the rapidly heated sample. In Fig. 7, the contribution of these parameters to the overall uncertainty of the specific electrical resistivity is provided as an example.

To quantify the uncertainty of the specific heat capacity of the pulse-heating experiments, the guidance of Matus [9] was followed. For the values of the change of volume, change of density, specific electrical resistivity including volume expansion, and thermal conductivity, an uncertainty consistent with the GUM has yet to be calculated. According to the GUM, the uncertainties reported in Table 5 are expanded relative uncertainties with a coverage factor of $k = 2$. The uncertainty bars are depicted within the figures.

6 Conclusion

In this study, the temperature dependences in the range from 500 to 2,650 K for a full set of thermophysical data (specific heat capacity, specific enthalpy, specific electrical resistivity, change of volume and density, thermal conductivity, and thermal diffusivity) of the chromium–nickel–molybdenum steel DIN 1.4435 are reported. The literature data used for comparison do not correspond to exactly the same steel composition but rather to the similar stainless steel 316. The data show good agreement within the uncertainties of the literature values for the solid phase. For the liquid range, new data

Table 3 Uncertainties for the measured and calculated data. (Properties not marked with DSC are from pulse-heating experiments)

Physical properties	Uncertainty ($k=2$) (%)
Density at room temperature	±0.1
$H(T)$ in the solid phase, DSC	±5
$H(T)$ in the solid phase	±7
$H(T)$ in the liquid phase	±4
ΔH at melting	±28
$\rho_{IG}(T)$ in the solid phase	±2.2
$\rho_{IG}(T)$ in the liquid phase	±1.8
$c_p(T)$ in the solid phase, DSC: <1,200 K/>1,200 K	±3/±5
$c_p(T)$ in the solid phase	±6.5
$c_p(T)$ in the liquid phase	±2.5
$a(T)$ in the solid phase, DSC: <1,200 K/>1,200 K	±5/±8.5
$a(T)$ in the solid phase	±8.3
$a(T)$ in the liquid phase	±4.4

are presented; literature values are only available within a few degrees of the melting point.

Acknowledgment This work was supported by the Austrian "Forschungsförderungsgesellschaft mbH", Sensengasse 1, 1090 Vienna, under Contract No. 810999.

References

1. B. Wilthan, C. Cagran, G. Pottlacher, Int. J. Thermophys. **26**, 1017 (2005)
2. C. Otter, G. Pottlacher, H. Jäger, Int. J. Thermophys. **17**, 987 (1996)
3. K. Mills, *Recommended Values of Thermophysical Properties for Selected Commercial Alloys* (ASM Int., Materials Park, Ohio, 2002), ISBN: 0-87170-753-5
4. T.K. Chu, C.Y. Ho, in *Proceedings of the 15th International Conference on Thermal Conductivity*, Ottawa, Canada (Plenum Press, New York, 1978), pp. 79–104
5. R.D. Pehlke, A. Jeyarajan, H. Wada, *Summary of Thermal Properties for Casting Alloys and Mold Materials* (University of Michigan, National Technical Information Service (STI), 1982)
6. P.G. Klemens, R.K. Williams, Int. Metals Rev. **31**, 197 (1986)
7. B. Wilthan, C. Cagran, C. Brunner, G. Pottlacher, Thermochim. Acta **415**, 47 (2004)
8. Deutsches Institut für Normung e.V. DIN. *Leitfaden zur Angabe der Unsicherheit beim Messen*. Beuth Verlag GmbH, 1st edn., 1995; original: *Guide to the Expression of Uncertainty in Measurement* (ISO, Geneva, Switzerland, 1993)
9. M. Matus, Technisches Messen **72,** 584 (2005), ISSN: 0171-8096